# Supplementary Information for "X-ray Fluorescence Standing Wave Study of the Interaction of the Antimicrobial Peptide Indolicidin with a Supported Model Membrane", Basnet. *et. al.*

## 1 X-ray Reflectivity Model and Fitting Procedure

X-ray reflectivity measurements were performed on both neat phospholipid bilayers and bilayers incubated with gold nanoparticle-labeled indolicidin. These measurements were analyzed using a slab model, where the bilayer, substrate and water overlayer are represented as stacks of uniform slabs with fixed x-ray scattering length density. The x-ray scattering length density is approximately equal to the electron density but contains small adjustments for energy dependent anomalous scattering. Each slab was characterized by three parameters: its thickness ($d$), electron density ($\rho$), and the roughness of its top interface ($\sigma$). The roughness was defined as the square root of the variance of surface height fluctuations over the correlation length of the X-ray beam.

The topmost and bottommost layers in the model were, by necesssity, treated differently. The top layer, representing the bulk solvent, was assumed to extend infinitely upward and therefore had no defined thickness or top surface roughness, leaving only its electron density as a parameter. Similarly, the bottommost layer, representing the silicon substrate, was assumed to extend infinitely downward and thus had no defined thickness, with only its roughness and electron density as parameters. Since both the top and bottom layers correspond to bulk materials with well-known electron densities, their densities were not varied but instead held fixed at the known values for bulk water and bulk silicon. All other layers in the model had three adjustable parameters.

In X-ray reflectivity when the beam enters from above, it undergoes refraction at the solvent interface. However, in this study, the X-rays entered from the side, eliminating the need for a refraction correction. As a result, the incident angle within the bulk solvent was identical to the external incident angle.

Reflectivity from the parameterized model was calculated using the Parratt

formalism [1], and the model parameters were optimized to fit the experimental reflectivity data via non-linear least-squares fitting using the Python `lmfit` package [2]. The best-fit parameters for the neat phospholipid bilayer are presented in Table 2, while those for the bilayer incubated with gold-nanoparticle-labeled indolicidin are shown in Table 3. The model consisted of seven slabs: (1) water, (2) distal headgroup, (3) combined tailgroup, (4) proximal headgroup, (5) $SiO_2$, (6) SiO, and (7) Si. The bilayer components were modeled with the nominal chemical composition of $CH_2$. Chemical mass densities (in $g/cm^3$) were converted to electron densities (in $e^-/nm^{-3}$) using material-specific conversion factors (see Table 1). Modeling in terms of chemical compositions and mass densities allows more accurate accounting for the imaginary component of the complex dielectric constant. Although this component was likely negligible for the current fitting, the computational framework was implemented to support this formalism.

Table 1: Conversion factors from mass density ($g/cm^3$) to electron density ($e^-/nm^{-3}$).

| Material | Conversion Factor |
|---|---|
| Water | 0.3345 |
| $CH_2$ | 0.343 |
| $SiO_2$ | 0.301 |
| Si | 0.307 |

The substrate parameters were based on the results of Steinrück [3] and Vega [4], who both found that introducing a 0.15 nm SiO layer between the silicon and $SiO_2$ layers significantly improved fits for supported films on oxidized silicon substrates. Although this interfacial layer has its greatest impact at wavevectors higher than those probed in the present study, we included it—with fixed parameters—to enhance model accuracy without adding free variables. The limited $Q$-range of the data does not support independent determination of all layer roughnesses, thicknesses, and densities. To avoid overparameterization, selected parameters were fixed at physically reasonable values for phospholipid bilayers. These non-varied parameters are denoted with an asterisk (*) in the fit results table.

For the bilayer prepared from liposomes incubated with gold-labeled indolicidin, uncertainties in several fitted parameters exceed their nominal best-fit values. This behavior suggests that decomposing the bilayer into discrete layers with independently varying thicknesses, densities, and roughnesses likely overparameterizes the model. In this case, however, it was not straightforward to impose additional constraints, as the structural impact of the gold-labeled indolicidin is not easily predicted. We therefore emphasize the real-space electron density profile as a more robust and interpretable outcome than the individual fit parameters. Since the substrate is unaffected by the addition of indolicidin, we fixed the substrate parameters to the values obtained from the fit to the neat

bilayer. Given that the bilayer structure in this sample is inferred almost entirely from a weak Kiessig fringe that rapidly decay with increasing wavevector, the data primarily support the conclusion that the bilayer is significantly more disordered than the neat bilayer. The detailed shape of the electron density profile does not represent a unique structural solution given the limited information content of the reflectivity data.

| **Material** | **density (g/cc)** | **Thickness (nm)** | **Surface Roughness (nm)** |
|---|---|---|---|
| Water ($H_2O$) | 1.00 | (–) | (–) |
| Headgroup ($CH_2$) | 1.5 (*) | 0.74 ± 0.3 | 0.83 ± 0.3 |
| Tailgroup ($CH_2$) | 0.71 (*) | 3.47± 0.2 | 0.56 ± 0.07 |
| Headgroup ($CH_2$) | 1.5 (*) | 0.43 ± 0.1 | 0.34 ± 0.06 |
| $SiO_2$ | 2.2 (*) | 1.23 (0.1) | 0.15 ± .1 |
| SiO | 1.86 (*) | 0.15 (*) | 0.15 (*) |
| Si | 2.3 (*) | (–) | 0.15 (*) |

Table 2: Best-fit parameters for the phopholipid bilayer without indolicidin (neat). Here (–) indicates that the parameter has no value, (e.g. thickness and roughness of the top layer) and (*) indicates a fixed parameter. Parameters without error bars were held fixed during fitting.

| **Material** | **density (g/cc)** | **Thickness (nm)** | **Surface Roughness (nm)** |
|---|---|---|---|
| Water ($H_2O$) | 1.00 | (–) | (–) |
| Headgroup ($CH_2$) | 1.81 ± 0.07 | 0.78 ± 0.1 | 1.02 ± 0.04 |
| Tailgroup ($CH_2$) | 0.56 ± 0.06 | 3.38 ± 0.6 | 1.50 ± 0.1 |
| Headgroup ($CH_2$) | 1.07 ± 0.9 | 0.57 ± 0.5 | 0.57 ± 0.15 |
| $SiO_2$ | 2.2 (*) | .56(*) | 0.10 (*) |
| SiO | 1.86 (*) | 0.15 (*) | 0.15 (*) |
| Si | 2.3 (*) | (–) | 0.15 (*) |

Table 3: Best-fit parameters for the phopholipid bilayer with gold labeled indolicidin. Here (–) indicates that the parameter has no value, (e.g. thickness and roughness of the top layer) and (*) indicates a fixed parameter. Parameters without error bars were held fixed during fitting.

## 2 Fit to Multilayer

Accurately modeling the electric field intensity of the standing wave requires a well-characterized reflectivity model for the multilayer crystal. Here we describe

in detail the properties of the crystal and the model used to simulate the x-ray reflectivity.

The multilayer was fabricated via chemical vapor deposition at the Argonne Optics facility. The base substrate was a highly polished and flat Si crystal obtained from Coastline Optics, with a nominal rms surface roughness of 0.1 nm. A Ti binding layer was then deposited onto the crystal. This was followed by 20 Mo/Si bilayers (Mo on top, Si underneath), and capped with a Si overlayer. All depositions were done in vacuum, but after removing the multilayer from vacuum the top Si layer was exposed to air, leading to the formation of an oxide layer. An oxide layer also formed on the top of the base silicon crystal which was exposed to air before deposition. In order to accurately model the topmost silicon oxide layer the model includes a transition region between Si and $SiO_2$, as modeled in Vega *et al.* [4] and Steinruck *et al.* [3]. The full multilayer structure is:

$$\mathrm{Air/SiO_2/SiO_x/Si/(Mo/Si)_{20X}/Ti/SiO_2/Si}$$

To refine the layer thicknesses and interfacial roughnesses, a reflectivity model was constructed using the Parratt formalism and fit to experimental X-ray reflectivity measurements taken in air with a fixed-tube X-ray source at Northern Illinois University. The detailed multilayer parameters are presented in Table 4. Due to the large number of parameters, not all could be fully constrained by the reflectivity data alone. Assumptions based on the fabrication process were used to fix certain values at plausible estimates. The layer spacings, interfacial roughness, and Mo/Si fraction within each bilayer were best constrained by the positions of the higher-order Bragg peaks (not shown). The remaining parameters were varied to optimize the fit between zero angle and the first two Bragg peaks, while others were held fixed. Error bars for the varied parameters are shown in Tab. 4

Figure 1 shows the reflectivity in the region between zero angle and the first Bragg peak. The final fit has a reduced $\chi^2 = 78$, indicating deviations larger than experimental error bars. However, it accurately reproduces the Bragg peak position and width. The fit is also highly sensitive to the Si overlayer height, which sets the spacing between the multilayer and the sample surface. This is due to the strong dependence of the reflectivity minimum at $\theta = 0.3^\circ$ to this parameter. The sensitivity to this parameter is specifically addressed by showing the variation of the reflectivity model when the overlayer height is manually adjusted by $\pm 1$ nm and $\pm 2$ nm (green and blue lines in figure).

# 3 X-ray Standing Wave Fluorescence Calculation

The reflectivity model for the multilayer structure was used to simulate the electric field distribution responsible for the x-ray standing wave. The standing wave arises from the interference between the downward- and upward-propagating

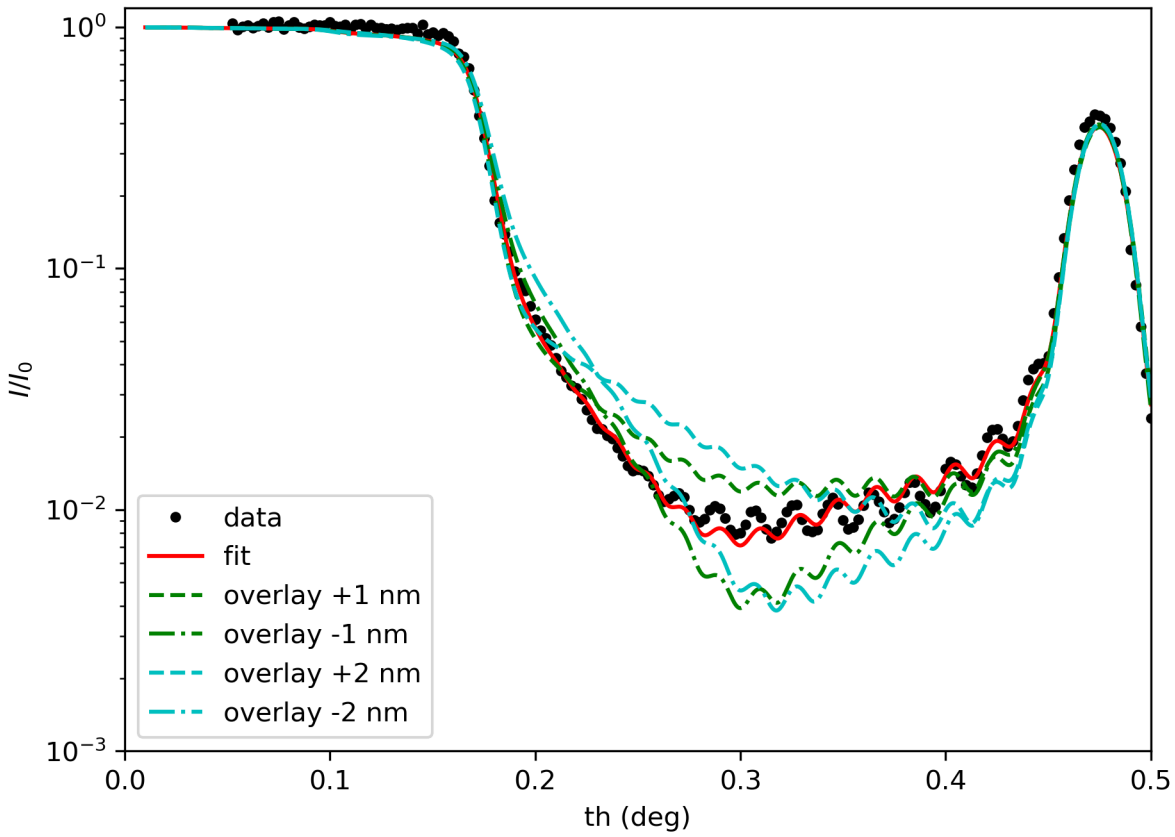


Figure 1: X-ray reflectivity from the multilayer in air compared to the fitted model. The dashed green and blue lines show the fit when the overlayer height is manually adjusted by ±1 nm and ±2 nm.

Table 4: Multilayer Model Parameters

| **Material** | **Electron Density ($nm^{-3}$)** | **Thickness (nm)** | **Surface Roughness (nm)** |
|---|---|---|---|
| Air | 0 | – | – |
| $SiO_2$ | 663 | 1.0 | 0.3 |
| $SiO_x$ | 560 | 0.15 | 0.15 |
| Si | 702 | 4.6 ± 0.06 | 3 |
| Mo | 2544 | 3.10 ± 0.05 | 0.77 ± 0.03 |
| Si | 702 | 1.48 ± 0.03 | 0.34 ± 0.04 |
| | | (Repeated 20 times) | |
| Ti | 1261 | 10.4 ± 0.1 | 0.3 |
| $SiO_2$ | 663 | 3.0 | 0.3 |
| Si | 702 | – | 0.3 |

components of the x-ray field within and above the multilayer. These fields are computed using custom Python code implemented in the `pySWXF` package [5].

For each slab in the multilayer model, the electric field is represented as a superposition of a downward-propagating plane wave with wavevector component $k_{z,i}$ and an upward-propagating wave with wavevector $-k_{z,i}$. The complex transmission and reflection amplitudes within each layer, denoted $T_i$ and $R_i$ respectively, are calculated using the Parratt recursion formalism [6], following the treatment in Tolan [7].

The total electric field within slab $i$ at position $z$ is given by

$$E_i(z) = T_i e^{-ik_{z,i}z} + R_i e^{ik_{z,i}z}, \tag{1}$$

and the corresponding standing wave intensity is

$$I_i(z) = |E_i(z)|^2.$$

This formalism naturally accounts for the interference pattern generated near the Bragg condition, and allows computation of the electric field intensity profile above the sample surface as a function of incident angle. The implementation of this calculation is contained in the `standing_wave` subroutine within the `refl_funs` submodule of the `pySWXF` package.

# 4 Characterization of liposome solution

Liposomes were prepared using the ethanol injection method and then extruded 21 times through a 100-nm pore-size polycarbonate membrane filter. The expected 100 nm liposome extrusion size was verified using a Brookhaven Instruments Dynamic Light Scattering spectrometer. The resulting size distribution, as determined from an intensity weighted log normal distribution is shown below.

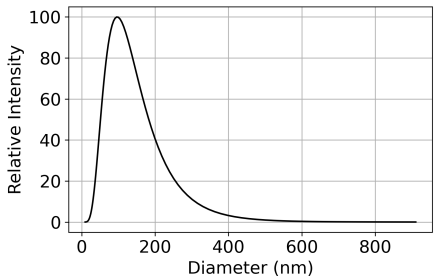


Figure 2: Distribution of Liposome Sizes from Dynamic Light Scattering

# 5 Comparison of One, Three, and Five Layer Fits

Figs. 3, 4 and 5 show the fits to the measured fluorescence vs. angle and the resulting real-space profiles for the 10 $\mu$M, 5 $\mu$M, and 2 $\mu$M samples.

For all three samples, the three layer fits appear to be optimal. The single-layer fits perform poorly in capturing the data, whereas the five-layer fits appear underconstrained and exhibit excessively large error bars.

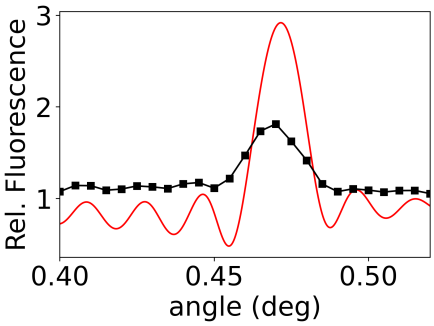


(a) 10 $\mu$M 1-layer fit

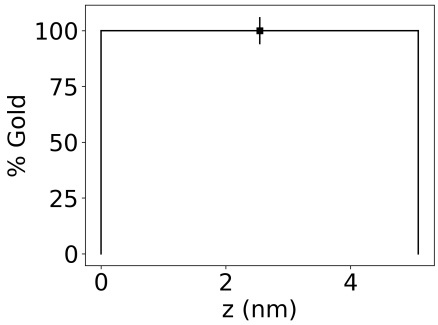


(b) 10 $\mu$M 1-layer profile

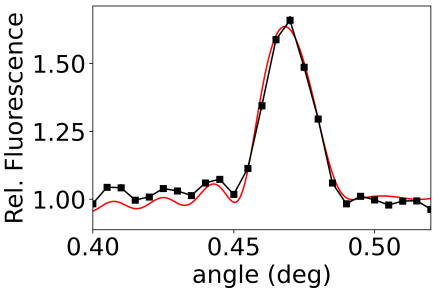


(c) 10 $\mu$M 3-layer fit

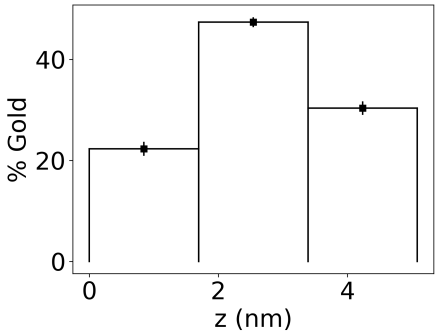


(d) 10 $\mu$M 3-layer profile

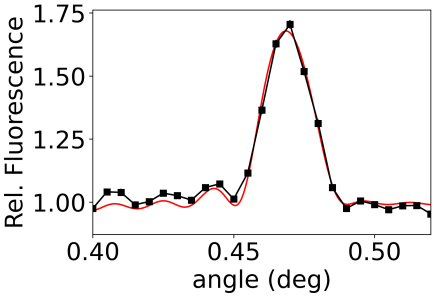


(e) 10 $\mu$M 5-layer fit

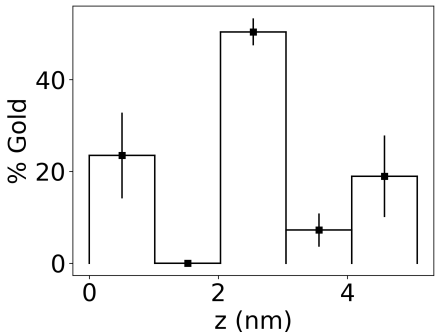


(f) 10 $\mu$M 5-layer profile

Figure 3: Fits and corresponding real-space profiles for the 10 $\mu$M sample.

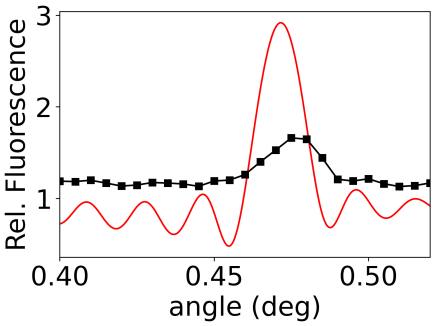


(a) 5 $\mu$M 1-layer fit

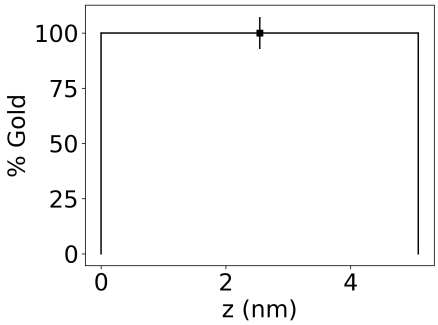


(b) 5 $\mu$M 1-layer profile

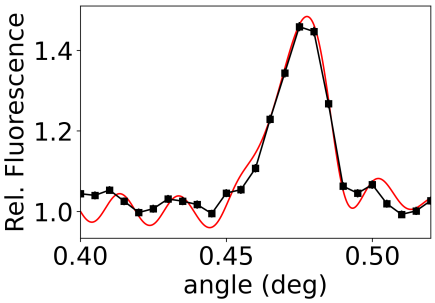


(c) 5 $\mu$M 3-layer fit

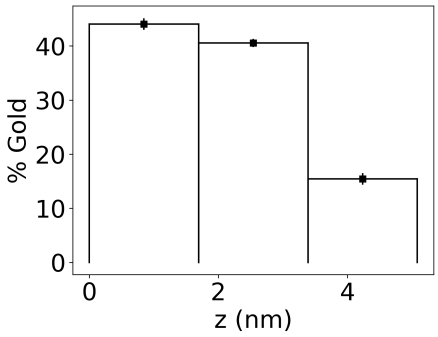


(d) 5 $\mu$M 3-layer profile

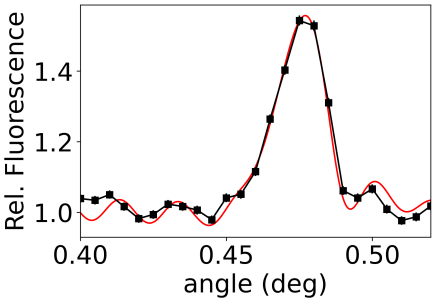


(e) 5 $\mu$M 5-layer fit

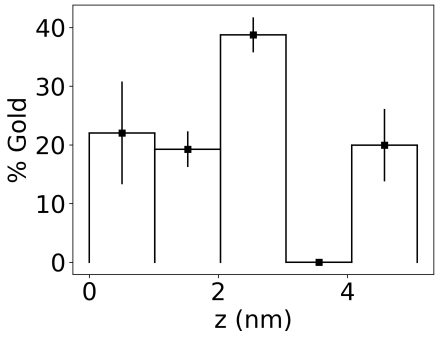


(f) 5 $\mu$M 5-layer profile

Figure 4: Fits and corresponding real-space profiles for the 5 $\mu$M sample.

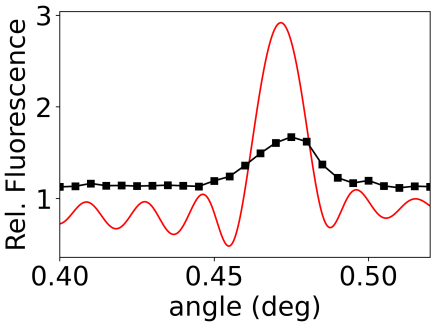


(a) 2 $\mu$M 1-layer fit

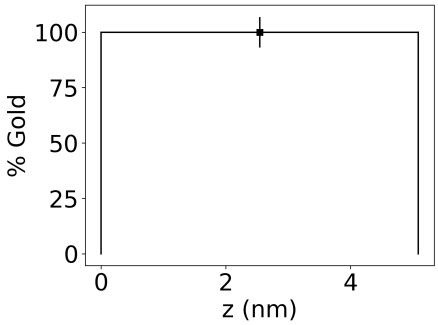


(b) 2 $\mu$M 1-layer profile

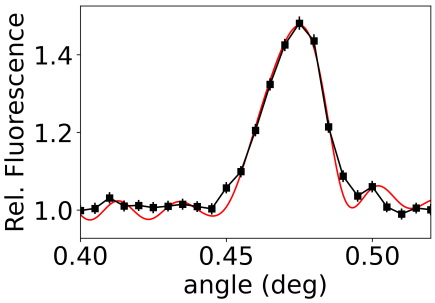


(c) 2 $\mu$M 3-layer fit

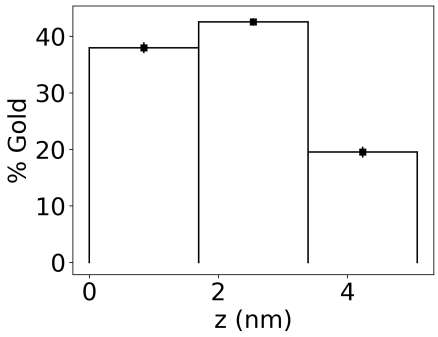


(d) 2 $\mu$M 3-layer profile

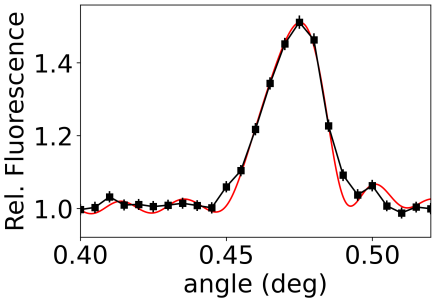


(e) 2 $\mu$M 5-layer fit

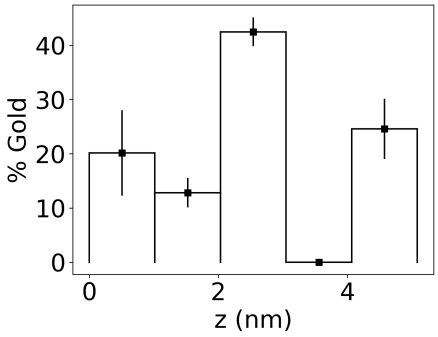


(f) 2 $\mu$M 5-layer profile

Figure 5: Fits and corresponding real-space profiles for the 2 $\mu$M sample.

# References


[1] Metin Tolan. *X-Ray Scattering from Soft-Matter Thin Films*, volume 148. 2000.

[2] Matthew Newville et al. Lmfit: Non-linear least-square minimization and curve-fitting for python, 2014.

[3] Hans Georg Steinrück, Andreas Schiener, Torben Schindler, Johannes Will, Andreas Magerl, Oleg Konovalov, Giovanni Li Destri, Oliver H. Seeck, Markus Mezger, Julia Haddad, Moshe Deutsch, Antonio Checco, and Benjamin M. Ocko. Nanoscale structure of si/sio2/organics interfaces. *ACS Nano*, 8:12676–12681, 12 2014.

[4] Michael Vega, Laurence Lurio, Jyotsana Lal, Evguenia A. Karapetrova, and Elizabeth R. Gaillard. Structure of supported dppc/cholesterol bilayers studied via x-ray reflectivity. *Phys. Chem. Chem. Phys.*, 22:19089–19099, 2020.

[5] L. B. Lurio. pySWXF: Code for calculating reflectivity and standing wave x-ray reflectivity. `https://pypi.org/project/pySWXF/`, 2025. Accessed: 2025-05-08.

[6] L. G. Parratt. Surface studies of solids by total reflection of x-rays. *Physical Review*, 95(2):359–369, July 1954.

[7] Metin Tolan. X-ray and neutron reflectivity. *Zeitschrift für Kristallographie - Crystalline Materials*, 213(6):319–336, 1998.